AIP | The Journal of Chemical Physics

Experimental and modeling study of the ion-molecule association reaction H 3 O + + H 2 O (+ M) → H 5 O 2 + (+ M)

S. Hamon, T. Speck, J. B. A. Mitchell, B. Rowe, and J. Troe

Citation: The Journal of Chemical Physics **123**, 054303 (2005); doi: 10.1063/1.1935520
View online: http://dx.doi.org/10.1063/1.1935520
View Table of Contents: http://scitation.aip.org/content/aip/journal/jcp/123/5?ver=pdfcov
Published by the AIP Publishing

Articles you may be interested in

Growth of polyphenyls via ion–molecule reactions: An experimental and theoretical mechanistic study
J. Chem. Phys. **138**, 204310 (2013); 10.1063/1.4807486

Growth of polyaromatic molecules via ion-molecule reactions: An experimental and theoretical mechanistic study
J. Chem. Phys. **133**, 184308 (2010); 10.1063/1.3505553

The study of state-selected ion-molecule reactions using the vacuum ultraviolet pulsed field ionization-photoion technique
J. Chem. Phys. **125**, 132306 (2006); 10.1063/1.2207609

Experimental and theoretical study of the ion–molecule association reaction NH 4 + + NH 3 (+ M)→ N 2 H 7 + (+ M)
J. Chem. Phys. **117**, 2557 (2002); 10.1063/1.1491409

Theoretical mechanistic study on the ion–molecule reactions of CCN + / CNC + with H 2 O and HCO + / HOC + with HCN/HNC
J. Chem. Phys. **116**, 1892 (2002); 10.1063/1.1431272

Reuse of AIP Publishing content is subject to the terms: https://publishing.aip.org/authors/rights-and-permissions. Downloaded to IP: 134.76.223.157 On: Thu, 07 Jul 2016 08:14:50

HTML ABSTRACT + LINKS

Experimental and modeling study of the ion-molecule association reaction $H_3O^+ + H_2O(+M) \rightarrow H_5O_2^+(+M)$

S. Hamon,[a] T. Speck,[b] J. B. A. Mitchell, and B. Rowe
Physique des Atomes, Lasers, Molécules, et Surfaces, Unité Mixte de Recherche (UMR), 6627 du Centre National de la Recherche Scientifique (CNRS), Université de Rennes 1, 35042 Rennes, France

J. Troe[c]
Institut für Physikalische Chemie, Universität Göttingen, Tammannstrasse 6, D-37077 Göttingen, Germany

(Received 1 March 2005; accepted 25 April 2005; published online 5 August 2005)

Experimental results for the rate of the association reaction $H_3O^+ + H_2O(+M) \rightarrow H_5O_2^+(+M)$ obtained with the Cinétique de Réactions en Ecoulement Supersonique Uniforme flow technique are reported. The reaction was studied in the bath gases $M = He$ and N_2, over the temperature range of 23–170 K, and at pressures between 0.16 and 3.1 mbar. At the highest temperatures, the reaction was found to be close to the limiting low-pressure termolecular range, whereas the limiting high-pressure bimolecular range was approached at the lowest temperatures. Whereas the low-pressure rate coefficients can satisfactorily be reproduced by standard unimolecular rate theory, the derived high-pressure rate coefficients in the bath gas He at the lowest temperatures are found to be markedly smaller than given by simple ion-dipole capture theory. This result differs from previous observations on the related reaction $NH_4^+ + NH_3(+M) \rightarrow N_2H_7^+(+M)$. This observation is tentatively attributed to more pronounced contributions of the valence part of the potential-energy surface to the reaction in $H_5O_2^+$ than in $N_2H_7^+$. Falloff curves of the reaction $H_3O^+ + H_2O(+M) \rightarrow H_5O_2^+(+M)$ are constructed over wide ranges of conditions and represented in compact analytical form.
© *2005 American Institute of Physics*. [DOI: 10.1063/1.1935520]

I. INTRODUCTION

$H_3O^+(H_2O)_n$ cluster ions are important constituents of the terrestrial atmosphere, cluster ions with $n=1$ particularly in the *D* region of the ionosphere (altitude 60–90 km).[1] Likewise, these species play an important role in interstellar clouds[2] or comets.[3] The formation and dissociation reactions of these species are of interest for a general understanding of the ion chemistry in these environments, see, e.g., Ref. 4. The present study concerns the formation of clusters with $n=1$, i.e., the reaction leading to proton-bound dimers of water $H_2O \cdot H^+ \cdot H_2O$ (i.e., $H_5O_2^+$). The reaction has been studied before under low-pressure conditions[5–8] where it proceeds as the termolecular process

$$H_3O^+ + H_2O(+M) \rightarrow H_5O_2^+(+M). \tag{1.1}$$

Bath gases $M = He$, Ar, H_2, O_2, N_2, and CH_4 were employed. Mostly experiments were carried out near 300 K, but temperatures between 300 and 570 K were also studied with the bath gas CH_4.[8] For a summary of measurements before 1976, see Ref. 7. As the molecular parameters of $H_5O_2^+$ such as the vibrational frequencies and the bond energy are becoming increasingly well known from *ab initio* calculations[9–11] and from experiments,[12–14] it appears tempting now to interpret the rate coefficients of the association reaction in its low-pressure termolecular range in terms of standard unimolecular rate theory, e.g., in the version of Ref. 15.

Measurements of the formation rate of $H_5O_2^+$ in the high-pressure bimolecular range, or at least in the falloff region connecting up to this range, so far have not been reported. However, there is some interest in this range not only in order to arrive at a complete characterization of reaction (1.1) but also because the association of H_3O^+ with H_2O constitutes the first step of the important proton exchange reaction

$$H_3O^+ + H_2O \rightarrow H_2O + H_3O^+. \tag{1.2}$$

Being of interest for proton transfer in a variety of environments, this process recently has been modeled on a reduced dimensionality *ab initio* potential-energy surface.[16] A comparison with experimental results for the high-pressure limiting association rate of reaction (1.1) would be meaningful. With improving characterization of the potential, a more detailed theoretical modeling should also become feasible in the near future.

With decreasing temperature, the transition between low-pressure termolecular and high-pressure bimolecular association of reaction (1.1) is expected to shift to lower pressures. We have experimentally demonstrated this behavior[17] for the related formation of proton-bound dimers of ammonia,

$$NH_4^+ + NH_3(+M) \rightarrow N_2H_7^+(+M). \tag{1.3}$$

In experiments between 15 and 170 K at bath gas concentrations of the order of 10^{16}–10^{17} molecule cm^{-3} the re-

[a]Present address: 1 Avenue Robert Schumann, 33700 Merignac, France.
[b]Present address: 15 Allée des Orchidées, 92220 Bagneux, France.
[c]Electronic mail: shoff@gwdg.de

 © 2005 American Institute of Physics

Reuse of AIP Publishing content is subject to the terms: https://publishing.aip.org/authors/rights-and-permissions. Downloaded to IP: 134.76.223.157 On: Thu, 07 Jul 2016 08:14:50

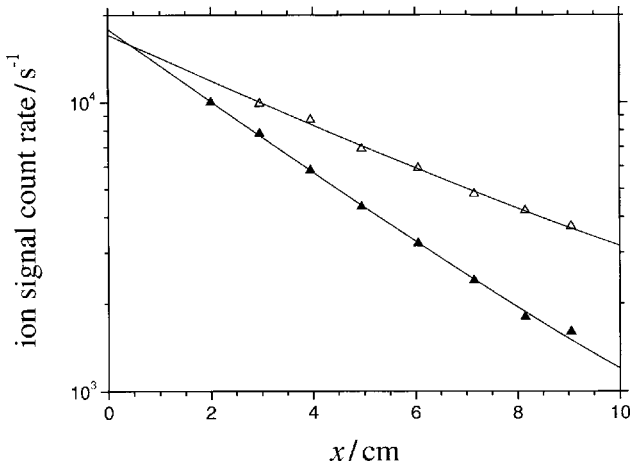

FIG. 1. Decrease of the H_3O^+ signal as a function of the downstream position x (▲: $[H_2O]=1.2\times10^{14}$ molecule cm^{-3}, △: $[H_2O]=8.7\times10^{13}$ molecule cm^{-3}, $T=157.5$ K).

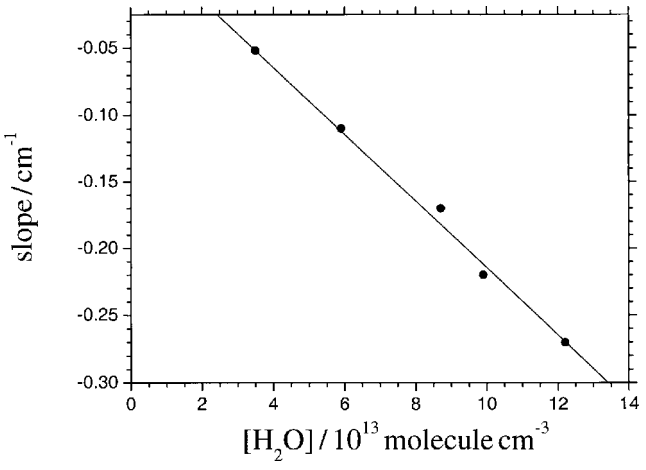

FIG. 2. Slopes of Fig. 1 as a function of $[H_2O]$ ($T=157.5$ K).

action was shown to change from conditions near to the high-pressure limit (at 15 K) to conditions near to the low-pressure limit (at 170 K). A set of falloff curves could be constructed which was consistent with standard unimolecular rate theory. In the present work we applied the same approach to reaction (1.1), i.e., we again used the experimental Cinétique de Réactions en Ecoulement Supersonique Uniforme (CRESU) flow technique and we tried to model the results by standard unimolecular rate theory. Whereas the experiments gave quite comparable results as for reaction (1.3), the modeling met with unexpected difficulties. After describing our experimental results, in the present work we try to understand the encountered modeling problems.

II. EXPERIMENTAL RESULTS

In the present work we used again the CRESU technique[17–20] in which a continuous supersonic flow is created by expanding the carrier gas of the reaction through a Laval nozzle. Each of the carefully designed nozzles generates downstream one temperature T and one bath gas pressure P (or bath gas concentration $[M]$). Before entering the expansion nozzle, small concentrations of the reactant are introduced into the carrier gas. In the present case, H_2O was introduced by passing the carrier gas through a saturator filled with liquid H_2O. The H_3O^+ ions were formed at the exit of the nozzle by crossing the flow by a 10-keV, 10 -μA electron beam. The concentrations of H_3O^+ were then followed along the flow by a mobile mass spectrometer. The concentrations of H_2O essentially stayed constant over the distance used for the measurements.

The H_3O^+ concentrations decayed exponentially with distance along the flow as demonstrated in Fig. 1 for two H_2O concentrations. The slopes of plots like Fig. 1 then were plotted as a function of $[H_2O]$, see Fig. 2. Employing the known flow velocity v, these results then were converted into second-order rate coefficients k_{rec} through

$$\frac{d[H_3O^+]}{dx} = -\frac{k_{rec}}{v}[H_3O^+][H_2O]. \tag{2.1}$$

The employed method of introduction of H_2O and determination of its concentration resulted in an uncertainty of k_{rec} of about ±50%. For further details of our experimental method, see Ref. 17.

Tables I and II summarize our measurements of k_{rec} in the bath gases He and N_2. Since each condition (T and $[M]$) required the use of a different nozzle, only a limited number of measurements could be made. However, we achieved measurements over wide ranges of temperature, in the present study between about 23 and 170 K and over a certain range of bath gas concentrations.

Our earlier studies[17] of the formation of the proton-bound dimer of ammonia, Eq. (1.3), indicated that the pseudo-second-order rate coefficients k_{rec} corresponded to intermediate parts of the falloff curve between the limiting low- and high-pressure ranges of the reaction. We expected the same to be the case for the present reaction. For an ori-

TABLE I. Pseudo-second-order (k_{rec}) and pseudo-third-order ($k_{rec}/[He]$) rate coefficients of the reaction $H_3O^+ + H_2O(+He) \rightarrow H_5O_2^+(+He)$ (k_{rec}=experimental values, $k_{rec,\infty}$ extrapolated such as described in Sec. III C).

T/K	$[He]/10^{16}$ molecule cm^{-3}	$k_{rec}/10^{-9}$ cm^3 molecule^{-1} s^{-1}	$k_{rec}/10^{-26}$ [He] cm^6 molecule^{-2} s^{-1}	$k_{rec,\infty}/10^{-9}$ cm^3 molecule^{-1} s^{-1}
22.9	5.22	1.4	2.7	2.9
25.0	7.53	2.4	3.2	5.3
36.0	5.89	1.6	2.7	4.5
49.1	11.4	0.99	0.87	2.8
123.0	13.4	0.34	0.25	2.9
157.5	14.1	0.30	0.21	⋯

Reuse of AIP Publishing content is subject to the terms: https://publishing.aip.org/authors/rights-and-permissions. Downloaded to IP: 134.76.223.157 On: Thu, 07 Jul 2016 08:14:50

TABLE II. Pseudo-second-order (k_{rec}) and pseudo-third-order ($k_{rec}/[N_2]$) rate coefficients of the reaction $H_3O^+ + H_2O(+N_2) \rightarrow H_5O_2^+(+N_2)$ (k_{rec} =experimental values).

T/K	$[N_2]/10^{16}$ molecule cm^{-3}	$k_{rec}/10^{-9}$ cm^3 molecule^{-1} s^{-1}	$k_{rec}/10^{-26}$ $[N_2]$ cm^6 molecule^{-2} s^{-1}
47.7	2.73	4.6	17
74.5	1.69	1.7	10
84.6	1.63	1.8	11
169.7	0.56	0.16	2.8

entation, therefore, we first created third-order ($k_{rec}/[M]$ as a function of T) and second-order (k_{rec} as a function of T) plots of our results such as shown in Figs. 3 and 4.

Extrapolation of our third-order plots in Fig. 3, for M =He, to 300 K gave good agreement of $k_{rec}/[M]$ with earlier measurements from Refs. 6 and 7. The same was found for $M=N_2$.[5] It appears worth mentioning that measurements of $k_{rec}/[M]$ with $M=N_2$ and CH_4 at 300 K seem to agree but are about a factor of 5 larger than the results for M=He. For orientation purposes, we provide representations of the pseudo-third-order rate coefficients such as drawn by the lines in Fig. 3,

$$k_{rec}/[He] = 5.4 \times 10^{-28}(T/298\ \mathrm{K})^{-1.6}\ \mathrm{cm^6\ molecule^{-2}\ s^{-1}} \tag{2.2}$$

and

$$k_{rec}/[N_2] = 3.1 \times 10^{-27}(T/298\ \mathrm{K})^{-2.4}\ \mathrm{cm^6\ molecule^{-2}\ s^{-1}}. \tag{2.3}$$

However, we emphasize that these representations are misleading, since points at different positions of the falloff curve are combined, see below.

Figure 4 shows pseudo-second-order plots of k_{rec}. For orientation purposes, Fig. 4 also includes rate constants for ion-linear dipolar rotor capture such as given by the Su–Chesnavich equation.[21] One notices that all measured values of k_{rec} are below the corresponding Su–Chesnavich rate constants k_{SCh}. At low temperatures the measurements reach up to the order of magnitude of k_{SCh}, but nevertheless, always clearly stay below. The earlier measurements at temperatures of 300 K (and above) all were many orders of magnitude below the Su–Chesnavich values which suggests that they were done close to the limiting low-pressure termolecular range.

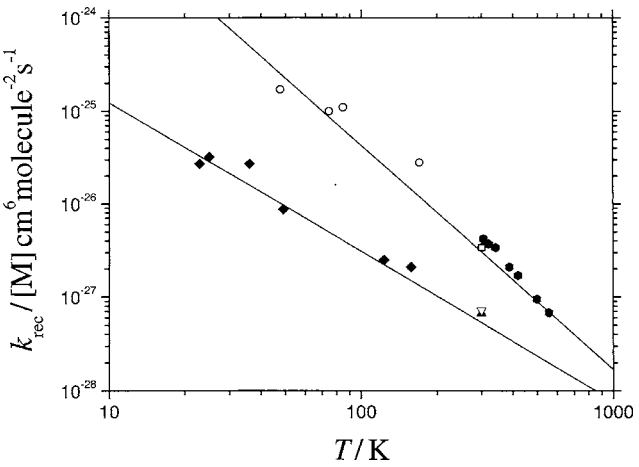

FIG. 3. Pseudo-third-order representation of the recombination rate coefficients k_{rec} in various bath gases M [◆: M=He from this work, ▽: M=He from Ref. 7, ▲: M=He from Ref. 6, ○: $M=N_2$ from this work, □: $M=N_2$ from Ref. 5, ⬣: $M=CH_4$ from Ref. 8, full lines: empirical representations by Eqs. (2.2) and (2.3) from this work].

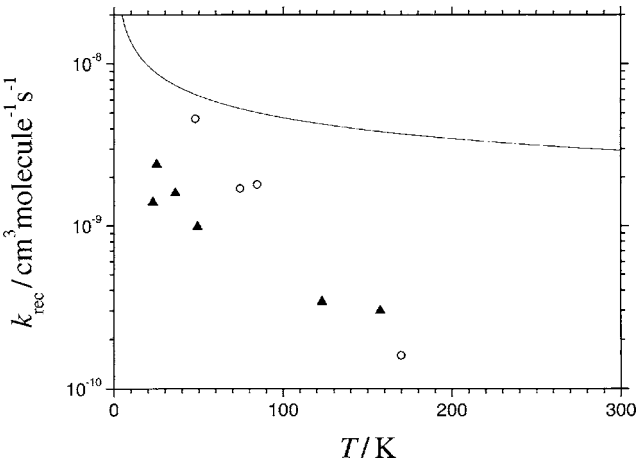

FIG. 4. Pseudo-second-order representation of the recombination rate coefficients k_{rec} in the bath gases He (▲) and N_2 (○) from this work (full line: Su–Chesnavich rate coefficient from Ref. 21 for ion-dipolar linear rotor capture, shown for orientation only).

III. MODELING OF RATE COEFFICIENTS

A. Limiting low-pressure rate coefficients

The pseudo-second-order plots of Fig. 4 strongly suggest that at least the available measurements near 300 K from Refs. 5–8 all correspond to conditions near to the low-pressure limit of the reaction. Therefore, at first we compare these measurements with modeling results from standard unimolecular rate theory. We use the formulation from Ref. 15 which, after conversion with the equilibrium constant, gives

$$k_{rec,0}/[M] \approx \beta_c Z \frac{\rho_{vib,h}(E_0) F_E kT F_{anh} F_{rot}}{Q_{vib}(H_2O) Q_{vib}(H_3O^+)} \times \frac{Q_{el,rot}(H_5O_2^+)}{Q_{el,rot}(H_2O) Q_{el,rot}(H_3O^+)} \left(\frac{h^2}{2\pi\mu kT}\right)^{3/2}, \tag{3.1}$$

where β_c denotes the collision efficiency which is related to the average energy $\langle \Delta E \rangle$ transferred per collision through $\beta_c/(1-\beta_c^{1/2}) \approx -\langle \Delta E \rangle / F_E kT$; Z is the relevant collision number per unit concentration such as given here by the Langevin collision number $Z_L = 2\pi q(\alpha/\mu)^{1/2}$ with the polarizability α of M; and $Q_{el,vib,rot}$ are electronic, vibrational, and rotational partition functions, respectively. The other factors are used such as described in Ref. 15. In other words, $\rho_{vib,h}(E_0)$ denotes the harmonic vibrational density of states at the dissociation energy E_0, F_E accounts for the energy dependence of $\rho_{vib,h}(E)$, F_{anh} describes the anharmonicity in the vibrational density of states, and F_{rot} accounts for rotational effects such as $E_0(J)$ and rovibrational densities of states.

Reuse of AIP Publishing content is subject to the terms: https://publishing.aip.org/authors/rights-and-permissions. Downloaded to IP: 134.76.223.157 On: Thu, 07 Jul 2016 08:14:50

Appendix A summarizes the molecular parameters required for the calculation of $k_{rec,0}/[M]$. We employ the complete set of harmonic frequencies of $H_5O_2^+$ such as derived in Ref. 11 from *ab initio* calculations. There is considerable uncertainty about the anharmonicity factor F_{anh}, last but not least because of the strongly anharmonic proton transfer potential. Part of F_{anh} could be accounted for by using fundamental instead of harmonic frequencies. However, these are becoming only slowly available experimentally.[13] In addition, the extrapolation of energy levels to energies of the order of the dissociation energy of $H_5O_2^+$ remains uncertain. Therefore, for the time being, we employ harmonic frequencies and tentatively use an estimate of the anharmonicity factor of $F_{anh}=3.5$ like that obtained by extrapolation to the dissociation energy for H_2O_2 on an *ab initio* potential[22] (if harmonic and not fundamental frequencies are employed, see Ref. 23). The rotational factor F_{rot} requires knowledge of the centrifugal barriers $E_0(J)$. Based on *ab initio* results for the potential as a function of the O–O distance,[9,11] one concludes that centrifugal barriers in the relevant range of angular momenta (quantum number J) are governed by the long-range ion-dipole potential. In this case, the centrifugal barriers, seen from the side of H_3O^+ and H_2O, are equal to zero. This range corresponds to $J(J+1)\leqslant 2\mu_D q\mu/\hbar^2$ (μ=reduced mass, q=ionic charge, and μ_D=dipole moment). For larger J, $E_0(J)$ steeply rises, see Ref. 24. Employing the formulas from Ref. 15, the properties of $E_0(J)$ mean that F_{rot} is close to its maximum value $F_{rot,max}$ which would be obtained in the absence of centrifugal barriers. The collision efficiencies β_c are derived empirically by comparing modeled and measured values of $k_{rec,0}/[M]$. This leads to empirical values of the average energies $\langle\Delta E\rangle$ transferred per collision. In order to estimate the temperature dependence of β_c, we assume $\langle\Delta E\rangle$ is only very weakly dependent on the temperature like in neutral molecules.[25]

Comparing modeling and experiment, we keep in mind that the absolute values of $k_{rec,0}/[M]$ at 300 K contain several factors which remain uncertain and have to be fitted. However, once these factors are fitted, the temperature dependence of $k_{rec,0}/[M]$ can be predicted with a considerable degree of confidence. We first look at the experiments with $M=N_2$. The factors contributing to $k_{rec,0}/[M]$ are included in Appendix B. By comparison of modeling and experiments at 300 K, we conclude that β_c is not too far from unity, i.e., that energy transfer between $H_5O_2^+$ and N_2 approaches strong collisions. This conclusion appears reasonable in view of the fact that $H_5O_2^+$ like $N_2H_7^+$ forms strongly interacting complexes with N_2 in which energy is efficiently exchanged. The observation of only small differences of β_c between experiments in N_2 and CH_4 confirms this conclusion. However, the situation appears different for M=He where obviously collisions are weak and β_c (300 K)$\approx$0.2 corresponds to $\langle\Delta E\rangle/hc\approx -100$ cm^{-1} (average energy transfer often is expressed in cm^{-1} such that we include the product of Planck's constant h and the velocity of light c). This value is of the expected order of magnitude.[25,26] Based on the information on β_c and taking into account that $\langle\Delta E\rangle$ generally is only weakly dependent on T, we are able to extrapolate $k_{rec,0}/[M]$ from 300 K to lower temperatures. This is done in Fig. 5 for the bath gases He and N_2. Likewise, experiments in CH_4 for higher temperatures are compared with the modeling. We realize that the experimental values of $k_{rec,0}/[M]$ increasingly fall below the modeled values. We interpret this observation as an indication for increasing deviations from the low-pressure limit.

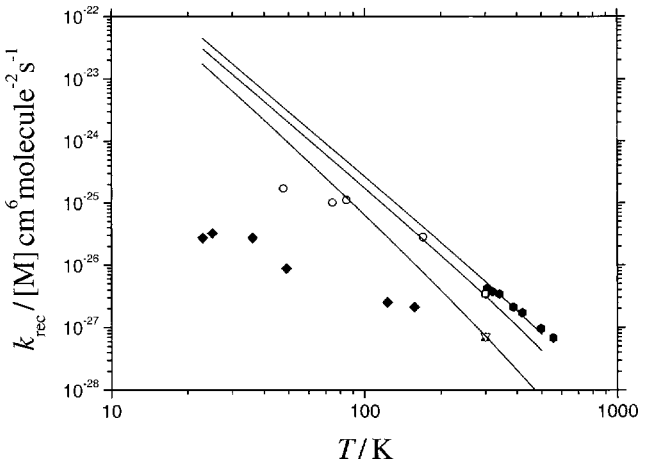

FIG. 5. Pseudo-third-order representation of the experimental results for $k_{rec}/[M]$ from Fig. 3 in comparison with modeled limiting low-pressure rate coefficients $k_{rec0}/[M]$ from this work, see text (symbols like in Fig. 3; lines from top to bottom: modeled $k_{rec0}/[M]$ for $M=CH_4$, N_2, and He, respectively).

B. Reduced falloff curves

After having modeled $k_{rec,0}/[M]$, we construct doubly reduced falloff curves $k_{rec}/k_{rec,\infty}$ as a function of the reduced concentration scale $k_{rec,0}/k_{rec,\infty}$ which is proportional to $[M]$. We perform this calculation in order to derive the high-pressure limiting value $k_{rec,\infty}$ of the second-order rate coefficient k_{rec} by combining extrapolated experimental $k_{rec,0}$ and measured k_{rec} in the falloff range. Reduced falloff curves in our approach are represented as

$$k_{rec}/k_{rec,\infty}=[x/(1+x)]F(x), \tag{3.2}$$

with $x=k_{rec,0}/k_{rec,\infty}$, see, e.g., Ref. 15. For strong collisions, $F(x)$ is represented as

$$F^{sc}(x)=(1+x)\int_0^\infty \sum_{J=0}^{\infty}(2J+1)[F_\rho F_W/(xF_\rho+F_W)] \times\exp(-E/kT)d(E/kT), \tag{3.3}$$

with a density-of-states factor

$$F_\rho=\rho(E,J)\Big/\int_{J=0}^{\infty}\sum_{J=0}^{\infty}(2J+1)\rho(E,J) \times\exp(-E/kT)d(E/kT) \tag{3.4}$$

and a number of activated complex states factor

$$F_W=W(E,J)\Big/\int_0^\infty \sum_{J=0}^{\infty}(2J+1)W(E,J) \times\exp(-E/kT)d(E/kT), \tag{3.5}$$

see Ref. 27. $\rho(E,J)$ denotes the rovibrational density of

Reuse of AIP Publishing content is subject to the terms: https://publishing.aip.org/authors/rights-and-permissions. Downloaded to IP: 134.76.223.157 On: Thu, 07 Jul 2016 08:14:50

TABLE III. Broadening factors $F(x)$ (including weak and strong collision broadening contributions) for $H_3O^+ + H_2O(+He) \rightarrow H_5O_2^+(+He)$ (see text).

T/K	$x=10^{-3}$	10^{-2}	10^{-1}	1	10	100	1000
22.9	0.98	0.83	0.46	0.26	0.30	0.43	0.56
25.0	0.97	0.81	0.43	0.25	0.30	0.43	0.55
36.0	0.94	0.69	0.36	0.22	0.28	0.42	0.54
49.1	0.90	0.61	0.33	0.22	0.28	0.41	0.54
123.0	0.76	0.53	0.31	0.21	0.27	0.40	0.53
157.5	0.74	0.53	0.31	0.20	0.27	0.40	0.53

states, and $W(E,J)$ is the number of activated complex states. The energy $E=0$ corresponds to separated H_3O^+ and H_2O. For low temperatures where only transitional modes contribute to $W(E,J)$ and, hence, to the shape of the reduced falloff curves, we employ the method described for $N_2H_7^+$ formation in Ref. 17. However, we also tested this simplified approach against a complete treatment accounting for conserved and transitional modes in $W(E,J)$, confirming the validity of the procedure for the low-temperature applications of relevance here. Our calculations are done completely by analogy to those described in Ref. 17 for the reaction $NH_4^+ + NH_3$, i.e., at this stage we assume that the number of activated complex states $W(E,J)$ is governed by a long-range ion-permanent dipole potential, see below. In addition, however, we account for the small additional broadening from weak collision contributions.

Table III summarizes broadening factors $F(x)$ as a function of $x=k_{rec,0}/k_{rec,\infty}$ and temperature T. The center broadening factors $F(x=1)$ are of similar magnitude as the corresponding values for the $N_2H_7^+$ system. Also, the complete broadening factors shown in Fig. 6 look similar as those of the $N_2H_7^+$ system. However, it remains to be seen whether broadening factors for ion-permanent dipole potentials adequately represent the present reaction system.

C. Experimental determination of limiting high-pressure rate coefficients

The observation that the experimental rate coefficients from Fig. 5 with decreasing temperature increasingly fall below the extrapolated $k_{rec,0}$ in the present work serves for the determination of $k_{rec,\infty}$. We use Eq. (3.2) in the implicit form

$$k_{rec,\infty} = k_{rec}(1+x)/xF(x), \tag{3.6}$$

with $x=k_{rec,0}/k_{rec,\infty}$. Equation (3.6) generally allows for a unique determination of $k_{rec,\infty}$ from the measured k_{rec} and $k_{rec,0}$. Only near to the center of the falloff curve, where $F(x)$ does not change much with x, the determination becomes not feasible. This was the case for all four experiments in $M=N_2$ and for the one experiment in $M=$He at 157.5 K. Table I includes the values for $k_{rec,\infty}$ from the experiments with $M=$He where $k_{rec,\infty}$ could be derived in the described way. Unfortunately, because of the given reasons, we are not able to exploit the experiments in $M=N_2$ for a derivation of $k_{rec,\infty}$.

Figure 7 compares the derived apparent values of $k_{rec,\infty}$ (open symbols), which are obtained from the experimental values of k_{rec} (filled symbols), with the rate coefficients from the Su–Chesnavich equation[21] (full line) for ion-dipolar linear rotor capture. We find that the derived points are systematically below the Su–Chesnavich capture rate coefficients k_{SCh}. We emphasize that the values of k_{SCh} at the present stage are given for orientation only, see below. Our observations differ from the corresponding results for the $N_2H_7^+$ system where, for the bath gas He, good agreement with the Su–Chesnavich equation was found over the range of 15–50 K. For that system, for the bath gas N_2, the derived

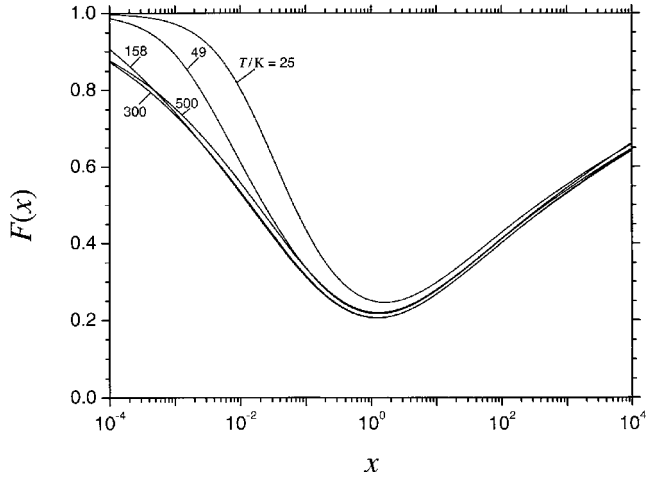

FIG. 6. Broadening factors $F(x)$ of falloff curves for $M=$He, see text.

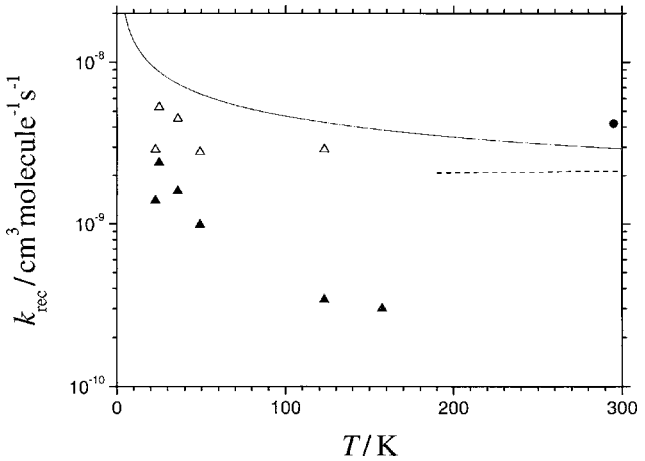

FIG. 7. Pseudo-second-order representation of the experimental results in the bath gas He for k_{rec} (▲: from this work) in comparison with extrapolated $k_{rec\infty}$ (△: from this work), experimental rate coefficients from isotope exchange (● from Ref. 31, multiplied by 2), calculated rate coefficients from proton transfer (---from Ref. 16, multiplied by 2), and Su–Chesnavich rate coefficients for ion-linear dipolar rotor capture (—from Ref. 21).

Reuse of AIP Publishing content is subject to the terms: https://publishing.aip.org/authors/rights-and-permissions. Downloaded to IP: 134.76.223.157 On: Thu, 07 Jul 2016 08:14:50

$k_{rec,\infty}$ over the range of 50–150 K were even found to be above k_{SCh}. This observation tentatively was attributed to $(NH_4^+)(N_2)_n$ clustering. In the following section possible reasons for the observed differences are discussed. Before doing this, we emphasize that the differences appear to be outside the experimental errors which are estimated to be about ±50%, see above.

D. Limiting high-pressure rate coefficients

In the following we speculate about the reasons for the differences between the values of $k_{rec,\infty}$ from the experiments and the Su–Chesnavich values. We first consider the data from experiments with M=He, where $k_{rec,\infty}$-values could be derived between 23 and 123 K. No temperature dependence of $k_{rec,\infty}$ was observed within the uncertainty of about ±50%, see Table I and Fig. 7. We obtained an average value of

$$k_{rec,\infty} = 3.7(\pm 1.8) \times 10^{-9} \text{ cm}^3 \text{ molecule}^{-1} \text{ s}^{-1}. \quad (3.7)$$

This value is markedly smaller than the Su–Chesnavich value of about $k_{SCh}=10\times10^{-9}$ cm^3 molecule^{-1} s^{-1} at 23 K, but essentially agrees with the value of about $k_{SCh}=4.5\times10^{-9}$ cm^3 molecule^{-1} s^{-1} at 123 K.

There are many possible reasons for deviations of $k_{rec,\infty}$ from k_{SCh}:

(i) The Su–Chesnavich equation only applies to capture of ions by permanent plus induced dipolar linear rotors. In the present case, however, the dipolar H_2O molecule is not linear but an asymmetric top. It was shown by statistical adiabatic channel model (SACM) calculations that symmetric-top[28] and asymmetric-top[29] capture rate constants k_{cap} can well be approximated by

$$k_{cap}/k_L \approx 1 + [k_{SCh}/k_L - 1]\exp[-(0.93/x)(B/A)^{1/2}], \quad (3.8)$$

with $k_L=2\pi q(\alpha/\mu)^{1/2}$ and $x=\mu_D(2\alpha kT)^{-1/2}$. In the present case one has $x\approx(8580 \text{ K/T})^{1/2}$ and $B/A \approx 1.28$ (Ref. 28) which leads to k_{cap} (23 K)$\approx 8.7\times10^{-9}$ in comparison with k_{SCh} (23 K)$\approx 9.1\times10^{-9}$ cm^3 molecule^{-1} s^{-1}. The corresponding values for T=123, 200, and 300 K are $k_{cap}=3.9\times10^{-9}$, 3.1×10^{-9}, and 2.6×10^{-9} in comparison with $k_{SCh}=4.3\times10^{-9}$, 3.5×10^{-9}, and 2.9×10^{-9} cm^3 molecule^{-1} s^{-1}, respectively. This could well explain the value of $k_{rec,\infty}$ from Eq. (3.7) at 123 K, but not the values derived at lower temperatures.

(ii) The Su–Chesnavich equation as well as Eq. (3.8) only applies to classical conditions. There is a turnover of k_{cap} to temperature-independent values at low temperatures which has been treated by SACM methods in Ref. 28–30. In the low-temperature limit, $k_{cap}\approx 14.3\times10^{-9}$ cm^3 molecule^{-1} s^{-1} is obtained.[28,30] k_{cap} in the low-temperature range decreases below the classical value from Eq. (3.8). However, this decrease becomes noticeable only below 20 K (Ref. 28) such that the small values of $k_{rec,\infty}$, at 23 K cannot be explained by quantum effects.

(iii) The reduced falloff expressions from the previous section, which were used for the derivation of $k_{rec,\infty}$, may have been inadequate, underestimating the extent of broadening. Such effects may occur when there are nonexponential lifetime distributions of the excited adducts such as observed in classical trajectory calculations of excited H_2O_2.[22] However, it would be difficult to imagine that the factor of 3 difference between ion-dipole capture rates k_{cap} and $k_{rec,\infty}$ would arise from such effects; it would also be difficult to understand that these effects do matter at 23 K but not at 123 K.

(iv) The part of the potential-energy surface of $H_5O_2^+$, which is most relevant for the association kinetics, may differ from the long-range ion-dipolar asymmetric-top rotor type. On the one hand the attraction may be stronger than given by the ion-dipole potential, on the other hand the anisotropy may differ from that of the ion-dipole potential. Both effects may stem from an important valence contribution to the potential. For the time being we favor this explanation of the properties of $k_{rec,\infty}$ from Eq. (3.7) (absolute value and temperature dependence). In the following we present some evidence for this hypothesis.

The high-pressure limit of reaction (1.1) is directly related to the proton transfer reaction (1.2). At the same time, it is linked to isotope exchange reactions such as

$$H_3O^+ + D_2O \rightarrow H_2DO^+ + HDO \rightarrow HD_2O^+ + H_2O. \quad (3.9)$$

At 295 K, the rate coefficient for reaction (3.9) was measured to be 2.2×10^{-9} cm^3 molecule^{-1} s^{-1} (Refs. 31 and 32) whereas 2.0×10^{-9} cm^3 molecule^{-1} s^{-1} was found for the reaction $D_3O^+ + H_2O$. Product distributions in both cases were also determined and found to be statistical, i.e., 2:1 for HDO:H_2O. The reduced dimensionality calculations of the rate for the proton transfer $H_3O^+ + H_2O$, Eq. (1.2), from Ref. 16 on the *ab initio* potential from Ref. 9 gave similar values, being about 1.05×10^{-9} cm^3 molecule^{-1} s^{-1} between 200 and 500 K. Assuming that these processes all proceed through sufficiently long-lived $H_5O_2^+$ such that statistical behavior is achieved, apart from minor zero-point energy effects one may assume that the corresponding capture rates are about twice the isotope exchange rates. Combining the experimental data at 295 K from Ref. 31 with the prediction of a negligible temperature dependence of the rate from Ref. 16 brings the capture rates into very good agreement with our results for $k_{rec,\infty}$ between 23 and 123 K such as given in Eq. (3.7). The results have markedly different temperature dependence from ion-dipole capture rates although they roughly agree in magnitude (except at our lower temperatures). How could one explain the difference in the temperature dependences? Capture processes governed by valence potentials often have only small temperature dependences (if no temperature dependences from electronic fine-structure effects and no contributions from electrostatic long-range effects arise[33]). In order to confirm the validity of this interpretation, classical trajectory calculations of the capture process (1.1) on an *ab initio* potential should be made, following the

Reuse of AIP Publishing content is subject to the terms: https://publishing.aip.org/authors/rights-and-permissions. Downloaded to IP: 134.76.223.157 On: Thu, 07 Jul 2016 08:14:50

SACM/classical trajectory (CT) strategy, e.g., of Ref. 34. Such calculations today are feasible and appear highly desirable.

There remain some open questions. Why could the high-pressure limiting $k_{rec,\infty}$ of the formation of proton-bound dimers of ammonia, Eq. (1.3), well be identified with ion-dipole capture rates[17] while this does not appear to apply for the present system? The answer may be found in the more spherical potential around NH_4^+ in comparison with H_3O^+. In addition, the $H_5O_2^+$ bond is about 1.5 times stronger than the $N_2H_7^+$ bond which should make valence effects more pronounced in the $H_5O_2^+$ system than in the $N_2H_7^+$ system. Another point of concern are the large recombination rates in the bath gas N_2 below 100 K which cannot be accommodated for by the present falloff curves, see below. A similar observation was made for the ammonia system at $T < 150$ K. It was suggested in Ref. 17 that this effect is due to massive clustering of NH_4^+ by bath gas molecules N_2 at low temperatures which causes a change of the mechanism, i.e., which produces a transition into a saturated radical-complex (chaperone) mechanism. If this is true, then there will be an intermediate temperature situation where a transition from an essentially pressure-independent radical-complex mechanism (at lower temperatures) to a pressure-dependent energy-transfer mechanism (at higher temperatures) occurs. This kinetic situation has not been treated before. One should imagine that the present measurements in N_2 at $T < 100$ K also correspond to this change of mechanism, i.e., to the transition into a saturated radical-complex mechanism involving capture of H_2O by $(H_3O^+)(N_2)_n$ clusters.

IV. REPRESENTATION OF RATE DATA AND MODELED FALLOFF CURVES

The present experimental low-temperature data for the association reaction (1.1) can be combined with earlier low-pressure results at higher temperatures and represented in a compact form. We employ

$$k_{rec,\infty} = 3.7(\pm 1.8) \times 10^{-9} \text{ cm}^3 \text{ molecule}^{-1} \text{ s}^{-1}, \quad (4.1)$$

$$k_{rec,0} = [\text{He}]1.05(\pm 0.1) \times 10^{-27}(T/300 \text{ K})^{-4.0} \text{ cm}^6 \text{ molecule}^{-2} \text{ s}^{-1}, \quad (4.2)$$

$$k_{rec}/k_{rec,\infty} = [x/(1+x)]F(x) \quad \text{with } x = k_{rec,0}/k_{rec,\infty}, \quad (4.3)$$

and broadening factors $F(x)$ such as illustrated by Fig. 6. Analytical expressions for $F(x)$ are also available, see Ref. 35, employing the modeled center broadening factors $F_c = F(x=1) \approx 0.22(\pm 0.02)$ which are independent of temperature. In the simplest form, neglecting the asymmetry illustrated in Fig. 6, e.g., $F(x)$ is approximated by

$$F(x) \approx F_e^{1/\{1+[(\log x)/N]^2\}}, \quad (4.4)$$

with $N \approx 0.75 - 1.27 \log F_c$. $k_{rec,\infty}$ is also assumed to be independent of temperature. $k_{rec,0}$ has been fitted to the partly falloff-corrected experimental data over the range of 123–300 K in order to derive $\langle \Delta E \rangle$. Assuming temperature-independent $\langle \Delta E \rangle$ such as this is normally observed,[15] the temperature dependence of $k_{rec,0}$ then follows from the modeling. $k_{rec,\infty}$ was taken as the average of the extrapolated points from Fig. 7. For bath gases other than He, $k_{rec,0}$ is modeled as

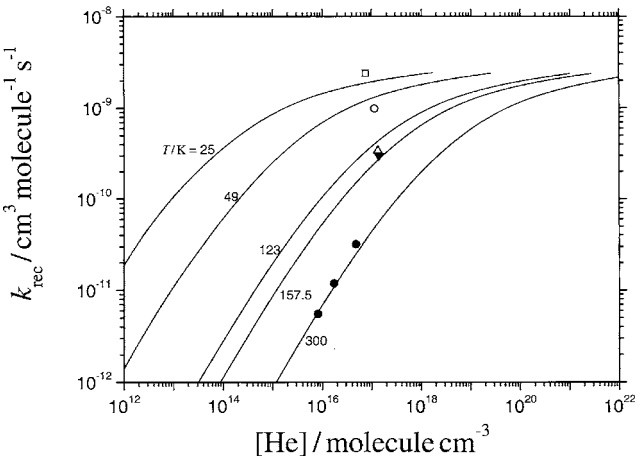

FIG. 8. Falloff curves for $H_3O^+ + H_2O(+He) \rightarrow H_5O_2^+(+He)$ [full lines modeling from this work with limiting rate coefficients from Sec. IV and $F(x)$ from Sec. III B, see also Table III; experimental points from this work, data for 300 K from Ref. 7, □: 25 K, ○: 49 K, △: 123 K, ▼: 157.5 K, and ●: 300 K].

$$k_{rec,0} = [N_2]5.1 \times 10^{-27}(T/300 \text{ K})^{-3.6} \text{ cm}^6 \text{ molecule}^{-2} \text{ s}^{-1}, \quad (4.5)$$

$$k_{rec,0} = [CH_4]2.1 \times 10^{-26}(T/300 \text{ K})^{-3.6} \text{ cm}^6 \text{ molecule}^{-2} \text{ s}^{-1}. \quad (4.6)$$

These expressions are fitted to low-pressure experimental points at $T > 150$ K in order to fix $\langle \Delta E \rangle$. The temperature coefficients then are modeled as described in Sec. III A.

The temperature coefficients in all three cases correspond to the range of 20–300 K. For 300–500 K they change to about −4.4 for $M = $He and −3.9 for $M = N_2$ and CH_4. (The differences arise from different absolute values of $\langle \Delta E \rangle$ entering β_c.) One notices that the given expressions for $k_{rec,0}$ markedly differ from the expressions of Eqs. (3.2) and (3.3). Figure 8 compares the available experimental data for $M = $He with our modeled falloff curves [$F(x)$ from Table III]. There is good agreement for the experiments with $M = $He. While the representation by an energy-transfer mechanism applies for He at all temperatures, in other bath gases ion-bath gas clustering at low temperatures (below about 150 K with $M = N_2$) probably produces a change of the mechanism to a saturated radical-complex mechanism. This is the reason for the marked discrepancies between the modeled falloff curves of Fig. 9 and the experimental points for $M = N_2$ from the present work.

V. CONCLUSIONS

Our measurements have provided data which allow for an analysis of the hydronium-water association reaction in terms of unimolecular rate theory. The importance of the potential-energy surface for the understanding of the high-pressure range is elucidated. There is ample evidence for an

Reuse of AIP Publishing content is subject to the terms: https://publishing.aip.org/authors/rights-and-permissions. Downloaded to IP: 134.76.223.157 On: Thu, 07 Jul 2016 08:14:50

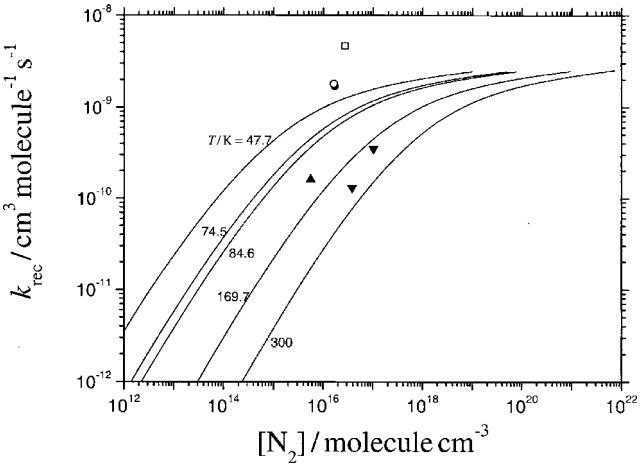

FIG. 9. As Fig. 8, but for the bath gas N_2 (experimental points from this work, data for 300 K from Ref. 5, □: 47.7 K, ●: 74.5 K, ○: 84.6 K, ▲: 169.7 K, and ▼: 300 K).

expectation that the high-pressure capture process is not dominated by ion-dipole forces but by contributions from the valence part of the potential. Capture calculations on an *ab initio* potential now appear feasible and are highly desirable. However, so far the *ab initio* potentials are not sufficiently complete, in particular, with respect to their multidimensional anisotropy, to allow for a meaningful analysis of this type. On the other hand, standard unimolecular rate theory very well reproduces low-pressure rate coefficients governed by the energy-transfer mechanism of the reaction.

ACKNOWLEDGMENTS

Financial support of this work by the Deutsche Forschungsgemeinschaft, the "Programme National: Physique et Chimie du Milieu Interstellaire," and the TMR network "Astrophysical Chemistry" of the European Community (No. ERB-FMRX-CT97-0132) is gratefully acknowledged. Discussions of this work with J. Bowman, J. Sauer, and A. Viggiano have also been most helpful.

APPENDIX A: MOLECULAR PARAMETERS

$H_5O_2^+$. Harmonic frequencies in cm^{-1} (Ref. 11): 3868, 3854, 3806, 3766, 1787, 1746, 1596, 1505, 794, 650, 577, 561, 481, 296, and 241; rotational constants in cm^{-1} (Ref. 12) 6.120, 0.2936, and 0.2923; $E_0/hc=11\,555$ cm^{-1} (Ref. 11), see also Ref. 36; and $\sigma=2$.

H_3O^+. Fundamental frequencies in cm^{-1} (Refs. 11, 37, and 38): 3468 [average of $\nu_1(+)$ and $\nu_1(-)$], 768 [average of $\nu_2(+)$ and $\nu_2(-)$], 3536, 3574, 1626, and 1694; rotational constants in cm^{-1} (Ref. 39) 11.444, 11.444, and 6.989; and $\sigma=3$.

H_2O. Fundamental frequencies in cm^{-1} (Ref. 11): 1590, 3641, and 3735; rotational constants in cm^{-1} (Ref. 39): 27.885, 14.512, and 9.281; $\sigma=2$; $\mu_D=1.85$ D; and $\alpha=1.444\times10^{-24}$ cm^3.

M. Polarizabilities α in 10^{-24} cm^3 (Ref. 40): 0.205 (He), 1.75 (N_2), and 2.56 (CH_4).

APPENDIX B: FACTORS IN THE LOW-PRESSURE RATE COEFFICIENTS $k_{rec,0}$

$M=$He: $Z_L=5.58\times10^{-10}$ cm^3 molecule^{-1} s^{-1}, $\rho_{vib,h}(E_0)=1.12\times10^4/\text{cm}^{-1}$, Whitten–Rabinovitch factor $a(E_0)=0.86$, $F_{anh}=3.5$ [estimated, for $\rho_{vib,h}(E_0)$ from harmonic (not fundamental) frequencies], $F_{rot}\approx F_{rot,max}$, and $\langle\Delta E\rangle/hc=-100$ cm^{-1} (estimated). $M=N_2$: $Z_L=7.76\times10^{-10}$ cm^3 molecule^{-1} s^{-1}, and $\langle\Delta E\rangle/hc=-1000$ cm^{-1} (estimated). $M=CH_4$: $Z_L=1.12\times10^{-9}$ cm^3 molecule^{-1} s^{-1}, and $\langle\Delta E\rangle/hc=-2000$ cm^{-1} (estimated).

T/K	β_c	F_E	$F_{rot,max}$	$k_{rec,0}$/[He] 10^{-26} cm^6 molecule^{-2} s^{-1}
25.0	0.75	1.01	781	1860
49.1	0.62	1.02	284	150
123.0	0.40	1.06	71.6	4.20
157.5	0.35	1.08	49.4	1.56
300.0	0.22	1.16	18.8	0.109
500.0	0.14	1.29	8.73	0.0115

$k_{rec,0}/[N_2]$ 10^{-26} cm^6 molecule^{-2} s^{-1}=315, 52, 0.48, 0.065, and $k_{rec,0}/[CH_4]$ 10^{-26} cm^6 molecule^{-2} s^{-1}=465, 83, 0.81, 0.06, for T=50, 150, 300, and 500 K, respectively.

[1] R. S. Narcisi and A. D. Bailey, J. Geophys. Res. **70**, 3687 (1965); E. E. Ferguson and F. Arnold, Acc. Chem. Res. **14**, 327 (1981); M. D. Perkins and F. L. Eisele, J. Geophys. Res. **80**, 9649 (1984); A. A. Viggiano and F. Arnold, in *Atmospheric Electrodynamics*, edited by H. Volland (CRC, Boca Raton, FL, 1995); E. E. Ferguson, F. C. Fehsenfeld, and D. L. Albritton, in *Gas Phase Ion Chemistry*, edited by M. T. Bowers (Academic, San Diego, 1979); G. Brasseur and S. Solomon, *Aeronomy of the Middle Atmosphere*, 2nd ed. (D. Reidel, Boston, 1986).
[2] E. Herbst, D. Smith, N. G. Adams, and B. J. Mc Intosh, J. Chem. Soc., Faraday Trans. 2 **85**, 1655 (1989); T. J. Millar, P. R. A. Farquahr, and K. Willacy, Astron. Astrophys., Suppl. Ser. **121**, 139 (1997).
[3] J. F. Crifo, Astrophys. J. **391**, 336 (1992); R. M. Haeberli, K. Altwegg, H. Balsiger, and J. Geiss, Astron. Astrophys. **297**, 881 (1995).
[4] F. C. Fehsenfeld and E. E. Ferguson, J. Geophys. Res. **74**, 2217 (1969).
[5] A. Good, D. A. Durden, and P. Kebarle, J. Chem. Phys. **52**, 212 (1970).
[6] R. C. Bolden and N. D. Twiddy, Faraday Discuss. Chem. Soc. **53**, 192 (1972).
[7] V. M. Bierbaum, M. F. Golde, and F. Kaufman, J. Chem. Phys. **65**, 2715 (1976).
[8] M. Meot-Ner and F. H. Field, J. Am. Chem. Soc. **99**, 998 (1977).
[9] L. Ojamäe, I. Shavitt, and S. J. Singer, J. Chem. Phys. **109**, 5547 (1998).
[10] M. V. Vener, O. Kühn, and J. Sauer, J. Chem. Phys. **114**, 240 (2001).
[11] X. Huang, M. J. Braams, and J. M. Bowman, J. Chem. Phys. **122**, 044308 (2005).
[12] L. I. Yeh, M. Okumura, J. D. Myers, J. M. Price, and Y. T. Lee, J. Chem. Phys. **91**, 7319 (1989).
[13] L. I. Yeh, Y. T. Lee, and J. T. Hougen, J. Mol. Spectrosc. **164**, 473 (1994).
[14] K. R. Asmis, N. L. Pivonka, G. Santambrogio, M. Brümmer, C. Kaposta, D. M. Neumark, and L. Wöste, Science **299**, 1375 (2003).
[15] J. Troe, J. Phys. Chem. **83**, 114 (1979).
[16] J. Rheinecker, T. Xie, and J. M. Bowman, J. Chem. Phys. **120**, 7018 (2004).
[17] S. Hamon, T. Speck, J. B. A. Mitchell, B. R. Rowe, and J. Troe, J. Chem. Phys. **117**, 2557 (2002).
[18] I. W. M. Smith and B. R. Rowe, Acc. Chem. Res. **33**, 261 (2000).
[19] B. R. Rowe, G. Dupeyrat, J. B. Marquette, and P. Gaucherel, J. Chem. Phys. **80**, 4915 (1984).
[20] A. Canosa, S. D. Le Picard, S. Gougeon, C. Rebrion-Rowe, D. Travers, and B. R. Rowe, J. Chem. Phys. **115**, 6495 (2001).

Reuse of AIP Publishing content is subject to the terms: https://publishing.aip.org/authors/rights-and-permissions. Downloaded to IP: 134.76.223.157 On: Thu, 07 Jul 2016 08:14:50

[21] T. Su and W. J. Chesnavich, J. Chem. Phys. **76**, 5183 (1982).
[22] B. Kuhn, T. R. Rizzo, D. Luckhaus, M. Quack, and M. A. Suhm, J. Chem. Phys. **111**, 2565 (1999); D. Luckhaus, Habilitation thesis, ETH Zürich, 1998; J. Troe and V. G. Ushakov (unpublished).
[23] J. Troe, Chem. Phys. **190**, 381 (1995); R. F. Salzgeber, V. A. Mandelshtam, and C. Schlier, J. Chem. Phys. **110**, 3756 (1999).
[24] J. Troe, Chem. Phys. Lett. **122**, 425 (1985).
[25] J. Troe, Proc. Combust. Inst. **28**, 1463 (2000).
[26] J. Troe, A. A. Viggiano, and S. Williams, J. Phys. Chem. A **108**, 1574 (2004); A. I. Fernandez, A. A. Viggiano, Th. M. Miller, S. Williams, I. Dotan, J. V. Seeley, and J. Troe, *ibid.* **108**, 9652 (2004).
[27] J. Troe and V. G. Ushakov, Faraday Discuss. **119**, 145 (2001); C. J. Cobos and J. Troe, Z. Phys. Chem. (Munich) **217**, 1031 (2003).
[28] J. Troe, J. Chem. Phys. **105**, 6249 (1996).
[29] M. L. Dubernet and R. Mc Carroll, Z. Phys. D: At., Mol. Clusters **15**, 333 (1990).
[30] J. Troe, J. Chem. Phys. **87**, 2773 (1987).
[31] D. Smith, N. G. Adams, and M. J. Henchman, J. Chem. Phys. **72**, 4951 (1980).
[32] N. G. Adams, D. Smith, and J. J. Henchman, Int. J. Mass Spectrom. Ion Phys. **42**, 11 (1982).
[33] A. F. Wagner, Proc. Combust. Inst. **29**, 1173 (2002).
[34] L. H. Harding, J. Troe, and V. G. Ushakov, Phys. Chem. Chem. Phys. **2**, 631 (2000).
[35] J. Troe (unpublished).
[36] N. F. Dalleska, K. Honma, and P. B. Armentrout, J. Am. Chem. Soc. **115**, 12125 (1993).
[37] M. Gruebele, M. Polak, and R. J. Saykally, J. Chem. Phys. **87**, 3347 (1987).
[38] P. Verhoeve, M. Versluis, J. J. Ter Meulen, W. L. Meerts, and A. Dymanus, Chem. Phys. Lett. **161**, 195 (1989).
[39] M. W. Chase, J. Phys. Chem. Ref. Data **9**, 1 (1998).
[40] A. A. Radzig and B. M. Smirnov, *Reference Data on Atoms, Molecules, and Ions* (Springer, Berlin, 1985).

Reuse of AIP Publishing content is subject to the terms: https://publishing.aip.org/authors/rights-and-permissions. Downloaded to IP: 134.76.223.157 On: Thu, 07 Jul 2016 08:14:50